Europe PMC Funders Group
Author Manuscript
Nat Chem Biol. Author manuscript; available in PMC 2010 May 13.

Published in final edited form as:
Nat Chem Biol. 2009 September ; 5(9): 631–639. doi:10.1038/nchembio.195.

Synthetic partial agonists reveal key steps in IP_3 receptor activation

Ana M. Rossi[1,4], **Andrew M. Riley**[2,4], **Stephen C. Tovey**[1], **Taufiq-Ur-Rahman**[1], **Olivier Dellis**[1], **Emily J. A. Taylor**[1], **Valery G. Veresov**[3], **Barry V. L. Potter**[2,*], and **Colin W. Taylor**[1,*]

[1]Department of Pharmacology, University of Cambridge, Tennis Court Road, Cambridge, CB2 1PD, UK

[2]Wolfson Laboratory of Medicinal Chemistry, Department of Pharmacy and Pharmacology, University of Bath, Claverton Down, Bath, BA2 7AY, UK

[3]Department of Cell Biophysics, Institute of Biophysics and Cell Engineering, Minsk 220072, Academicheskaya St. 27, Belarus.

Abstract

Inositol 1,4,5-trisphosphate receptors (IP_3R) are ubiquitous intracellular Ca^{2+} channels. IP_3binding to the IP_3-binding core (IBC) near the N-terminal initiates conformational changes that lead to opening of a pore. The mechanisms are unresolved. We synthesized 2-*O*-modified IP_3 analogues that are partial agonists of IP_3R. These are like IP_3 in their interactions with the IBC, but they are less effective than IP_3 in rearranging the relationship between the IBC and N-terminal suppressor domain (SD), and they open the channel at slower rates. IP_3R with a mutation in the SD occupying a position similar to the 2-*O*-substituent of the partial agonists has a reduced open probability that is similar for full and partial agonists. Bulky or charged substituents from either the ligand or SD therefore block obligatory coupling of the IBC and SD. Analysis of ΔG for ligand binding shows that IP_3 is recognised by the IBC and conformational changes then propagate entirely via the SD to the pore.

Inositol 1,4,5-trisphosphate receptors (IP_3R) are ligand-gated channels. They are expressed in most animal cells and mediate release of Ca^{2+} from the endoplasmic reticulum in response to the many stimuli that evoke IP_3 formation. IP_3R are tetrameric, and each subunit of about 2700 residues has an IP_3-binding site near the N-terminus and six transmembrane domains (TMD) towards the C-terminus (Fig. 1a)1. The pore is formed by the last pair of TMD and the intervening loop, the pore-loop ("P-loop"), from all four subunits1. The structure of the pore is predicted to be broadly similar to the pores of other tetrameric P-loop channels, like bacterial K^+ channels, for which high-resolution structures are available2. IP_3 binds to a discrete part of the IP_3R, the IP_3-binding core (IBC, residues 224-604, Fig. 1a)3. Although the extreme N-terminus (residues 1-223) is not required for IP_3 binding, it decreases the affinity for IP_3 and has therefore been called the suppressor domain (SD)4. The SD is thought to be required for channel gating because IP_3 binds to IP_3R without an

---

*Correspondence should be addressed to C.W.T. (cwt1000@cam.ac.uk) or B.V.L.P (b.v.l.potter@bath.ac.uk) .
[4]These authors contributed equally to this work.

AUTHOR CONTRIBUTIONS A.M.R. (Cambridge), S.C.T., T-U-R, O.D. and E.J.A.T. completed the biology experiments. V.G.V. performed molecular modelling. A.M.R. (Bath) designed and synthesized the ligands and contributed to molecular modelling. B.V.L.P. (chemistry) and C.W.T. (biology) designed and coordinated the project. C.W.T. and A.M.R. (Cambridge) wrote the manuscript with input from the other authors. All authors discussed the results and commented on the manuscript.

COMPETING INTERESTS STATEMENT The authors declare that they have no competing financial interests.

Note: Supplementary information and chemical compound information is available on the Nature Chemical Biology website.

Europe PMC Funders Author Manuscripts
Europe PMC Funders Author Manuscripts

Europe PMC Funders Author Manuscripts

Europe PMC Funders Author Manuscripts

SD, but it no longer opens the pore4,5. However, the links between IP_3 binding and gating are not understood, and nor do we have a structure of the entire IP_3R at sufficient resolution to provide insight into these gating mechanisms1,6.

Activation of ligand-gated ion channels begins with agonist binding to a stable closed state and proceeds via many short-lived intermediates to a state in which the pore is open7. This activation may proceed entirely through a sequence of incremental changes in the receptor8 or be dominated by a single concerted transition between two stable conformations9. Agonists differ in both the strength of their binding (affinity) and in their ability to drive the receptor to its open state (efficacy)10. A ligand with reduced efficacy must occupy more receptors than a full agonist to evoke the same cellular response. Such partial agonists, by occupying receptors, diminish the response to a full agonist11. Partial agonists are particularly useful for exploring the mechanisms of receptor activation because they lie between full agonists and antagonists in their ability to activate receptors7,10. This is true for all receptors, but ligand-gated ion channels are uniquely amenable to such analyses because single-channel recording allows key conformational changes of single receptors to be determined with outstanding temporal resolution7.

For these ligand-gated ion channels, full and partial agonists may differ in either the frequency with which they cause the receptor to visit the fully active open state or they may stabilize different open states that mediate lesser ion fluxes. In both cases, a partial agonist evokes lesser activation. Two subtypes of ionotropic glutamate receptors (iGluR) illustrate the distinction. These receptors, which mediate most excitatory neurotransmission in the brain, are those for which the structural basis of efficacy has been most thoroughly explored12,13. For the AMPA subtype of iGluR, a series of partial agonists, which differ from each other by only a single atom, close the clam-like binding site to varying degrees, but less completely than do full agonists. Partial agonists thereby preferentially open the pore to states with lesser conductance12. For full and partial agonists of the NMDA subtype of iGluR, the conformational changes in the binding site are more subtly different. Both cause similar closure of the clam, and they fully open the pore, but the conformational changes proceed more slowly for partial agonists14,15.

Affinity and efficacy are distinguishable, but the two properties are not independent because energy provided by agonist binding drives the conformational changes that cause channel opening10,16,17. This “binding-gating problem” is a fundamental issue in pharmacology10, but it can also be turned to advantage because the interplay depends upon both the efficacy of the ligand and the presence of the parts of the receptor through which conformational changes must pass. The former because partial agonists divert less binding energy than full agonists into effective conformational changes; and the latter because receptors lacking essential domains are expected to be less able to divert binding energy into conformational changes (Fig. 1b). Analyses of the free energy changes for ligand binding ($\Delta G = -RT ln K_d$, where K_d is the equilibrium dissociation constant) can thus provide insight into the conformational changes evoked by agonist binding. Comparisons of ΔG for full and partial agonists, and for agonist binding to normal and truncated IP_3R, can therefore contribute to defining the links between IP_3 binding and opening of the pore.

Here we synthesize a new series of partial agonists of the IP_3R, and, in defining their properties, we identify a novel form of partial agonism that allows us to define key steps in IP_3R activation.

Europe PMC Funders Author Manuscripts

Europe PMC Funders Author Manuscripts

RESULTS

Synthesis of 2-*O*-modified analogues of IP_3

All high-affinity agonists of all IP_3R have structures equivalent to the vicinal 4,5-bisphosphate and 6-hydroxyl of IP_3 (Fig. 1c), but the axial 2-hydroxyl is not required18. The essential phosphate moieties interact predominantly with opposite sides of the clam-like IBC (P-4 with the β_2-domain, and P-5 with the ARM domain)3 (Fig. 1a), suggesting that agonists might close the clam in a manner reminiscent of glutamate binding to iGluR6,13.

In seeking to develop novel high-affinity ligands of IP_3R that might differ in efficacy, we focused on the 2-OH group of IP_3 because earlier structure-activity analyses had suggested that analogues modified at this position retain activity18. The X-ray structure of the IBC with IP_3 bound subsequently confirmed that the 2-OH group of IP_3 makes no significant contacts with the IBC3.

We began by preparing homo-dimers of IP_3 with linkers of various lengths (**2, 3** and **4** in Fig. 1c), aiming initially to define the separation of IP_3-binding sites within a tetrameric IP_3R. However, informed by our initial results19,20 and cognizant that dimeric cGMP is a partial agonist of a cGMP-gated cation channel21, we extended our work to include syntheses of additional 2-*O*-modified analogues (Fig. 1c) and an assessment of their efficacy.

The shortest IP_3 dimer (**2**) is a symmetrically substituted *N,N'*-diethyl urea, synthesized by cross-linking of a protected D-2-*O*-(2-aminoethyl)-IP_3 building block using bis(4-nitrophenyl) carbonate19. A modification of this synthetic method was used to synthesize hetero-dimers such as **5, 6** and **7**, in which the second IP_3 moiety is replaced by a different inositol phosphate or by inositol (Scheme 1). We also synthesised an $_L$-IP_3 homo-dimer (**8**, the enantiomer of **2**) (Scheme 1) and an IP_3-adamantane conjugate (**9**). The syntheses of 2-deoxy-IP_3 (**10**)22 and 2-*O*-(2-aminoethyl)-IP_3 (**11**)23 were reported previously. Details of the synthetic procedures and compound characterizations are provided in Supplementary Methods online.

2-*O*-modified IP_3 analogues are high-affinity agonists of IP_3R

We used a cell line that expresses only recombinant rat IP_3R1 (DT40-IP_3R1 cells)24 to measure Ca^{2+} release from intracellular stores, and IP_3R1 purified from rat cerebellum to measure IP_3 binding. These analyses show that homo-dimers of IP_3 linked through the 2-*O*-positions of the inositol rings are high-affinity agonists of IP_3R. The shortest dimer (**2**) (Fig. 1c) binds to IP_3R1 with greater affinity than IP_3 (Table 1 and Supplementary Fig. 1a online) and stimulates Ca^{2+} release from intracellular stores at lower concentrations than does IP_3 (Table 1 and Supplementary Fig. 1b online). **2** is the most potent inositol phosphate-based agonist so far identified.

A homo-dimer of L-IP_3 (**8**) is, as expected, inactive because L-IP_3 does not bind to the IBC18. However, homo-dimers of IP_3 with longer linkers (**3, 4**) also bind to IP_3R with greater affinity than IP_3, as do hetero-dimers in which IP_3 is linked to inositol (inositol-IP_3, **7**), an unrelated bulky hydrophobic group (adamantane-IP_3, **9**), or to an inositol phosphate that does not itself bind to the IBC (IP_3-IP_5, **6**; or IP_3-$_L$-IP_3, **5**) (Table 1). The latter (**5-7** and **9**) demonstrate that high-affinity binding of IP_3 dimers does not result from an interaction with a second specific IP_3-binding site, nor does it result from alternating association of the two IP_3 moieties with the IBC19. Furthermore, the two components of the dimer must be linked, because a high concentration of IP_5 (**12**, 10μM) had no effect on the Ca^{2+} release evoked by IP_3 or 2-deoxy-IP_3 (**10**) (Supplementary Fig. 1c online). We conclude that

addition of bulky or charged groups to the 2-*O*-position of IP_3 produces high-affinity agonists of the IP_3R.

A new family of partial agonists of IP_3R

Because a partial agonist less effectively activates its receptor than a full agonist, it must occupy more receptors to evoke the same cellular response11. In our Ca^{2+} release assays, where each ligand caused the same maximal Ca^{2+} release as IP_3 (Table 1), we can therefore gain some insight into the efficacy of a ligand by comparing the concentration that causes 50% of the maximal response (EC_{50}) with that which occupies 50% of the binding sites (K_d).

For each ligand, we compared the EC_{50}/K_d ratio using DT40-IP_3R1 cells for the functional assays24 (EC_{50}) and purified IP_3R1 to measure IP_3 binding (K_d). Our results suggest that **2** occupies more IP_3R than IP_3 to evoke the same Ca^{2+} release (**2** has a higher EC_{50}/K_d ratio, Fig. 2a and Table 1). This indicates that **2** may be a partial agonist. These characteristics, an increase in both affinity and EC_{50}/K_d ratio, are shared by very different 2-*O*-modified IP_3 analogues (Fig. 2a and Table 1). They do not, therefore, depend upon precise structural features: an IP_3 moiety that binds to the IBC and a 2-*O*-substitutent larger than adamantane (**9**) are sufficient to increase both the affinity and EC_{50}/K_d ratio.

The EC_{50}/K_d ratio for adenophostin A (AdA, **13**, Fig. 1c)25, another high-affinity agonist of IP_3R, is similar to that for IP_3 (Fig. 2a and Table 1). This is consistent with single channel analyses, where IP_3 and AdA cause the IP_3R to open to the same maximal single channel open probability (P_o, the fraction of time that each channel spends in its open state) (Fig. 2b and Supplementary Table 1 online)26. We conclude that IP_3 and AdA are full agonists of the IP_3R, whereas **2-7** and **9** appear to be partial agonists.

The results shown in Fig. 2c confirm that **2** must occupy more IP_3R than the full agonist, AdA, to evoke the same Ca^{2+} release. DT40-IP_3R1 cells were first pre-treated with concentrations of AdA or **2** that caused the same Ca^{2+} release (5.7 ± 1.0% and 5.4 ± 1.3% of the intracellular stores, respectively) and then stimulated with IP_3. More IP_3 is required to evoke further Ca^{2+} release after treatment with **2** than after AdA (EC_{50} = 44.4 ± 3.19 and 4.37 ± 0.18nM, respectively). This confirms that **2** occupies more IP_3R than AdA to evoke the same Ca^{2+} release.

Because the nuclear envelope is continuous with the endoplasmic reticulum26, we can use patch-clamp recording from the outer nuclear envelope of DT40-IP_3R1 cells to resolve the behaviour of single IP_3R. To both maximize the amplitude of the currents recorded and to avoid the complexity of feedback regulation of IP_3R by Ca^{2+} passing through them1, we used K^+ as the charge-carrier in these experiments26,27. Both the single channel K^+ conductance (γ_K) and the mean channel open time (τ_o) were the same for all agonists examined (Fig. 2b,d and Supplementary Table 1 online). The open state of the IP_3R thus appears to be similar whether it is evoked by binding of a full (AdA, IP_3 and **10**) or partial agonist (**2, 6** and **9**).

However, for IP_3R activated by maximal concentrations of AdA, IP_3 or **10**, P_o was higher than with **2, 6** or **9** (Fig. 2b,e and Supplementary Table 1 online). Increasing the concentration of **2** (from 0.5 to 10μM, Fig. 2b,e) did not further increase P_o, and after stimulation with a mixture of IP_3 and **2** (10μM of each) P_o was significantly less than with IP_3 alone (Fig. 2b and Supplementary Table 1 online). These analyses of single IP_3R confirm and extend the results obtained with Ca^{2+} release and binding assays (Table 1 and Fig. 2a). Analogues of IP_3 with bulky additions to the 2-*O*-position (**2-7** and **9**) are high-

Europe PMC Funders Author Manuscripts
Europe PMC Funders Author Manuscripts

Europe PMC Funders Author Manuscripts

Europe PMC Funders Author Manuscripts

affinity partial agonists of IP_3R1. Subsequent analyses of the mechanisms underlying these properties of the 2-*O*-substituted analogues focus on **2** (Fig. 1c).

Our single channel analysis shows that whereas τ_o is similar for all agonists (Supplementary Table 1 online), mean channel closed times (τ_c) were longer for the partial agonists (**2, 6** and **9**) than for full agonists (IP_3, AdA and **10**) (Fig. 2e and Supplementary Table 1 online). The latter, assuming a simplified activation scheme (Fig. 2e, Supplementary Methods online), reveals that the rate constant for channel opening ($\beta = 1/\tau_c$) with partial agonists is less than with full agonists. The 2-*O*-modified analogues are the first partial agonists of IP_3R for which the basis of their reduced efficacy has been established. They open the channel fully (Fig. 2b,d), the channel closes at the same rate whether it has a partial agonist or IP_3 bound (α in Fig. 2e), but the rate constant for channel opening (β) is lower for partial agonists (Fig. 2e and Supplementary Table 1 online). We conclude that these full and partial agonists drive the IP_3R into a similar open state, but the partial agonists do so less effectively.

Full and partial agonists differ in how they rearrange the IBC-SD

For IP_3R, conformational changes evoked by IP_3 binding to the IBC near the N-terminal must be transmitted to the pore formed by residues close to the C-terminal (Fig. 1a). Some of the energy provided by IP_3 binding is used to drive the opening of the pore. The K_d ($\Delta G = -RT ln K_d$) measured in a binding assay is therefore determined by both the strength of the contacts between IP_3 and the IBC ("intrinsic binding affinity")16 and the ensuing conformational changes10.

The IBC includes all the amino acid residues that contact IP_3 (Fig. 1a)3,28 and each 2-*O*-modified agonist (**2-7** and **9-11**) (Fig. 1c) retains the groups within IP_3 that interact with the IBC. Furthermore, each of these ligands binds with similar affinity to the IBC alone (Fig. 3a and Table 1). Because the full (IP_3) and partial agonists (**2-7, 9**) are both expected to make the same contacts with the IBC and are also observed to bind to it with similar affinity, we suggest that they do not differ in the binding energy they divert into changing the conformation of the IBC. This contrasts with AMPA receptors, where the clam-like binding site closes more fully with more efficacious agonists12,13. The distinction highlights two fundamentally different ways of reducing efficacy, a defining feature of all ligand-receptor interactions10. A partial agonist may fail to make optimal contacts with the binding site and so less effectively activate the receptor (e.g., AMPA receptors12), or it may impair onward transmission of conformational changes. Subsequent experiments demonstrate that our partial agonists (**2-7** and **9**) belong to the second category. They are thereby useful in defining the steps that follow IP_3 binding.

For all three IP_3R subtypes, IP_3 binds to the IBC with greater affinity than to either full-length IP_3R or the NT (Fig. 3a, Table 1 and Supplementary Table 2 online)28,29. The SD reduces the IP_3 binding affinity through its intramolecular interaction with the IBC28 and appears also to mediate communication between the IBC and pore4,5. We therefore examined the contribution of the SD to the conformational changes initiated by IP_3 via analysis of ΔG for ligand binding.

Removal of the SD increases the affinity of the NT for IP_3, but it has lesser effects on binding of the partial agonists (Table 1). Efficacy (reported by the EC_{50}/K_d ratio) and the difference in ΔG ($\Delta G = -RT ln K_d$) for binding to the IBC and NT ($\Delta\Delta G$) are inversely correlated (Fig. 3b). Because we suggest that each agonist contributes similar "intrinsic binding energy"16,17 through the similar interactions that each makes with the IBC (Table 1 and Supplementary Table 2 online), the different $\Delta\Delta G$ for binding of full and partial agonists to the NT must reflect the extent to which each uses binding energy to rearrange the relationship between the IBC and SD16,17,30. We conclude that full and partial agonists

Europe PMC Funders Author Manuscripts

Europe PMC Funders Author Manuscripts

differ minimally in their interactions with the IBC, but radically in how they rearrange its relationship with the SD.

Conformational changes pass from the IBC entirely via the SD to the pore

IP_3 binds only to a small contiguous sequence within the IP_3R, the IBC (Fig. 1a). Truncations of the IP_3R might therefore disconnect IP_3 binding from downstream conformational changes without directly perturbing the IP_3-binding site. These truncated IP_3R might then reveal, via analysis of ΔG for ligand binding, the parts of the IP_3R through which IP_3-evoked conformational changes must pass (Fig. 1b).

All full-length IP_3R subtypes bind IP_3 with only slightly lower affinity than the NT (ΔΔG *ca*. -3kJ/mol)28, whereas the NT and IBC differ more substantially in their affinities for IP_3 (*ca*. -6kJ/mol) (Table 1 and Supplementary Table 2 online). This suggests that the most costly conformational changes evoked by IP_3 occur within the NT (~6kJ/mol) with downstream events requiring less energy (~3kJ/mol) (Fig. 3c). Removing the SD from full-length IP_3R increases its affinity for IP_3 by an amount (≤ *ca*. - 9kJ/mol)4 consistent with uncoupling IP_3 binding from all the conformational changes downstream of the IBC (Fig. 3c). These analyses suggest that the IBC communicates with the rest of the IP_3R entirely via the SD.

A site within the first 340 residues of the IP_3R, which includes the SD, appears to interact with a short cytosolic loop linking TMD 4 and 5 (Fig. 3c). This interaction has been proposed to open the pore directly31,32. Disruption of this loop increases the affinity of the IP_3R for IP_3 by an amount (*ca*. -3kJ/mol)32 that matches the estimated cost of all conformational changes downstream of the SD (Fig. 3c).

These analyses corroborate our suggestion that conformational changes pass directly and exclusively from the IBC to the SD, and then perhaps directly to the TMD4-5 loop31,32.

Point mutations within the SD mimic partial agonists

Removal of the SD and additions to the 2-*O*-position of IP_3 similarly increase binding affinity (Table 1). The latter, we suggest, because the analogues evoke lesser conformational changes in the IP_3R. Both modifications also uncouple ligand binding from gating, although removal of the SD does so more completely4,5 than do the 2-*O* modifications to IP_3. We therefore speculated that 2-*O*-modified analogues partially mimic removal of the SD by disrupting its interaction with the IBC and that this causes both a decrease in efficacy and an increase in affinity.

The SD has a structure reminiscent of a hammer with a large head and short handle (described earlier as an “arm”)33 (Fig. 4a). Others33 have shown that removing the handle of the SD (residues 67-108) minimally affects IP_3 binding to the NT. But mutation of highly conserved residues on the surface of the head domain, most notably within the β2-β3 loop (loop 2)33, increases the affinity of the NT for IP_3. We therefore tested our hypothesis that 2-*O*-modified analogues of IP_3 disrupt the IBC-SD interface by mutagenesis of residues in the β2-β3 loop and of other residues nearby in the 3D structure of the SD (Fig. 4a). As reported33, several mutations increased the affinity of the NT for IP_3, with the most effective (V33K) almost mimicking the effect of removing the entire SD. Another mutation (K52E) had no effect (Supplementary Table 3 online)33. Furthermore, and consistent with our suggestion that 2-*O*-substituents of IP_3 disrupt the IBC-SD interaction, the effective mutations had lesser effects on binding of **2** to the NT (Fig. 4b and Supplementary Table 3 online). From these non-additive effects, we conclude that binding of **2** displaces the SD in a manner that mimics its removal or displacement by appropriate mutations.

Europe PMC Funders Author Manuscripts

Europe PMC Funders Author Manuscripts

Our results so far establish that the 2-*O*-substituents of the IP_3 analogues and appropriate point mutations within the SD cause similar increases in binding affinity. These effects mimic removal of the SD, leading us to conclude that they result from disrupted communication between the IBC and SD. Given that the 2-*O*-substituted analogues are partial agonists, and that the SD is required for IP_3 to gate the pore4,5, we speculated that the point mutations might further mimic the analogues and give IP_3R that even full agonists are unable to activate fully.

In DT40 cells expressing IP_3R1 mutated within the SD (Fig. 4a and Supplementary Fig. 2a,b online), IP_3 and **2** evoke Ca^{2+} release from permeabilized cells and activate IP_3R in nuclear patch-clamp recordings (Fig. 4c-e, Supplementary Fig. 2c online, and Supplementary Table 4 online). The properties of these interactions are consistent with our prediction that disrupting the IBC-SD interaction decreases efficacy and increases agonist affinity by blocking propagation of conformational changes from the IBC. In permeabilized DT40 cells expressing IP_3R1 with the V33K mutation (IP_3R1^{V33K}), IP_3 and **2** are equipotent (Supplementary Fig. 2c online), and in single channel recordings each has the same P_o (Fig. 4d,e). This P_o is similar to that observed for normal IP_3R stimulated with **2**, but lower than the P_o with IP_3 (Fig. 2b,e). The less effective mutations have lesser effects (Fig. 4c), consistent with our suggestion that they cause lesser disruption of the IBC-SD interaction.

The structures of the IBC-IP_3 and SD are known3,33 (Fig. 1a), but not the relationship between them34. We used protein-protein docking to identify a likely relationship between them (Supplementary Methods online). The three IP_3R subtypes differ in their affinities for IP_3, but their IBC share similar sequences and bind IP_3 with the same affinity28. A subtype-specific interaction between the IBC and SD determines the different affinities of the three full-length IP_3R28. Because the residues within the SD that confer these subtype-selective interactions28,33 are likely to lie at an IBC-SD interface, this criterion was used to select between possible models of the IBC-SD complex. Our proposed model (Fig. 5a,b and Supplementary Fig. 3 online) is consistent with the radius of the NT-IP_3 complex from small-angle X-ray scattering34. In this structure, four of the loops (loops 2 and 5, and part of loops 3 and 7)33 that link the β-strands of the SD interact primarily with loops from the β_2-domain of the IBC (Supplementary Fig. 3 online). Within this IBC-SD structure, the second IP_3 moiety of **2** lies close to several point mutations in the SD (V33K, D34R, R36E) that reduce efficacy (Supplementary Table 4 online), each lying on the putative IBC-SD interface (within loop 2). The same interface includes the other effective mutation (K127E, within loop 5), but not the ineffective one (K52E) (Fig. 5a,b and Supplementary Fig. 3c,d online).

We conclude that bulky or charged groups introduced into the IBC-SD interface by either the ligand or the SD disrupt essential communication between the IBC and SD and thereby reduce efficacy.

DISCUSSION

We have synthesized and characterized a family of partial agonists of IP_3R that differ minimally from full agonists in their interactions with the binding site (IBC), but which have reduced efficacy because they block an obligatory communication between the IBC and SD. These results define two fundamentally different routes to reduced efficacy. A partial agonist may fail to make optimal contacts with the ligand-binding site12,13,35. Alternatively, it may, as we have shown for our partial agonists of IP_3R, bind normally and then, through additional interactions, block onward transmission of essential conformational changes. These novel properties of our partial agonists allow us to show that the conformational changes initiated at the IBC pass entirely via the SD to the pore (Fig. 5c).

Europe PMC Funders Author Manuscripts

Europe PMC Funders Author Manuscripts

Our activation scheme is consistent with an earlier proposal that IP_3 minimally affects the structures of the three domains of the NT, but rearranges their relationships via flexible linking loops34 (Fig. 5c). We suggest that IP_3 first stabilizes interaction of the β_2 and ARM domains of the IBC by interacting with residues in each3,36. These interactions require the 4- and 5-phosphate groups of IP_3. The IBC then interacts with the SD (=β_1 in Fig. 5c) to give a compact structure34 that allows the SD alone to signal onwards to the pore, probably via its interaction with the TMD4-5 loop (Fig. 5c)32.

IP_3R are close relatives of ryanodine receptors (RyR), sharing most sequence similarity within their N-termini and pores. The likely structural similarities between the SD of IP_3R and the N-terminal of RyR suggests these regions may have similar functions in both families of intracellular Ca^{2+} channels33. Mutations that cause RyR to become dysfunctional in malignant hyperthermia, central core disease (RyR1) and catecholaminergic polymorphic ventricular tachycardia (RyR2) cluster in four regions that include the N-terminal and a region close to the pore37. Furthermore, 3D reconstructions of RyR have shown that activation is associated with major conformational changes within a region that includes the N-terminus38. For RyR1, the same region includes residues that interact with the dihydropyridine receptor, which is the major physiological regulator of RyR1. From structure-based sequence alignment36, it has been suggested that the SD surface opposite to that which we suggest contacts the IBC (Supplementary Fig. 3e,f online) is most conserved between IP_3R and RyR. We speculate that this may be the surface that communicates with the conserved pore region for both IP_3R and RyR.

The SD of an IP_3R activated by a partial agonist fully engages the structures that open the pore because an open IP_3R is the same whether activated by a full or partial agonist (Fig. 2b,d and Supplementary Table 1 online), but it does so less frequently than when activated by a full agonist (Fig. 5c). The many additional proteins that interact with the SD1,33 may exert their effects on IP_3R by targeting this essential link between IP_3 binding and channel opening.

In conclusion, we have synthesized a family of 2-*O*-modified analogues of IP_3 and shown they are partial agonists of IP_3R. IP_3 and these partial agonists interact similarly with the IBC, but the 2-*O*-substituents of the analogues block transmission of essential conformational changes from the IBC to the SD. The partial agonists thereby open the channel less effectively. This unusual form of partial agonism allows us to define two means whereby a ligand may have reduced efficacy: it may either fail to make optimal contacts with the binding site, or it may bind like a full agonist but then interfere with subsequent conformational changes. By combining mutagenesis of IP_3R with analyses of the effects of these novel partial agonists, we have shown that the major conformational changes evoked by IP_3 occur within the N-terminal and they pass to the pore entirely via the SD (Fig. 5c).

METHODS

Synthesis of ligands

Adenophostin A (AdA, **13**)39, inositol 1,3,4,5,6-pentakisphosphate (IP_5, **12**)40 , IP_3 dimers19 **2, 3** and **4**, D-2-deoxy-IP_3 (**10**)22, and 2-*O*-(2-aminoethyl)-IP_3 (**11**)23 were synthesized as previously reported. Details of the syntheses of compounds **5–9** are given in Supplementary Methods online. IP_3 was from American Radiolabeled Chemicals. [^{3}H]-IP_3 (18-23Ci/mmol) was from Amersham Biosciences.

Europe PMC Funders Author Manuscripts

Europe PMC Funders Author Manuscripts

Stable expression of IP_3R1 in DT40 cells

Rat IP_3R1 were stably expressed in DT40 cells in which the genes for all endogenous IP_3R had been disrupted41. The open reading frame42 of rat IP_3R1 was amplified by PCR using primers P6 and P7 and cloned as an *EcoR*I fragment into pcDNA3. The CMV promoter was replaced by the chicken β-actin hybrid promoter, excised from the vector pAneo41, to produce the construct pcDNA3-IP_3R1. QuikChange II XL site-directed mutagenesis kit (Stratagene) was used to introduce point mutations in rat IP_3R1, which had been previously cloned into the pENTR1A vector. The primers are listed in Supplementary Table 5 online. Mutated IP_3R1 was subcloned into pcDNA3.2 by recombination (Gateway, Invitrogen). The sequences of all full-length IP_3R constructs were confirmed. DT40 cells stably expressing IP_3R1 and its mutants were generated and cultured as described24. Expression of mutant IP_3R in DT40 cell lines was quantified by immunoblotting (Supplementary Fig. 2a,b online).

Functional assay of IP_3R1 in DT40 cells

A low-affinity Ca^{2+}-indicator (Magfluo-4) trapped within the intracellular Ca^{2+} stores was used to measure IP_3-evoked Ca^{2+} release24.

Cloning and mutagenesis of N-terminal fragments of IP_3R1

Appropriate regions of rat IP_3R1 were amplified by PCR from the full-length receptor clone lacking the S1 splice region ($S1^-$). Fragments are numbered by reference to the full-length ($S1^+$) rat IP_3R1 (Accession number NM_001007235). PCR used P1 and P2 primers for the fragment including residues 1-604 (NT), and P3 and P2 for residues 224–604 (IBC). Both P1 and P3 insert a thrombin-cleavage site. Fragments were ligated into the pTrcHisA vector at the *Xho*I/*Eco*RI sites (Invitrogen) to allow expression of N-terminally tagged His_6 proteins. Insertion of the S1 splice region into the IBC fragment used QuikChange mutagenesis kit with P4 and P5 primers. Mutagenesis of residues within the SD used the same kit. The primers are listed in Supplementary Tables 5 and 6 online. The sequences of all constructs were confirmed by DNA sequencing.

Expression of IP_3R1 fragments in bacteria

Constructs were transformed into *E. coli* BL21(DE3)43 and 1ml of the culture was grown overnight at 37°C in Luria-Bertani medium (LBM) with 50μg/ml ampicillin. The inoculum was cultured at 22°C in 100ml of LBM until the OD_{600} reached 1.0–1.5, isopropyl β-D-thiogalactoside (0.5mM) was added, and after 20h at 15°C, cells were harvested (5000x*g*, 5min). The pellet was resuspended in Tris/EDTA medium (TEM: 50mM Tris, 1mM EDTA, pH 8.3) supplemented with 10% PopCulture (Novagen), 1mM 2-mercaptoethanol and protease inhibitor cocktail (Sigma). The suspension was incubated with lysozyme (100μg/ml) and RNAase (10μg/ml) for 30min on ice, and the lysate was sonicated for 20s. After centrifugation (30,000x*g*, 60min), aliquots of supernatant were frozen in liquid nitrogen and stored at -80°C.

For immunoblotting, samples were loaded onto SDS-PAGE gels, transferred to Immobilon membranes (Millipore) and His_6-tagged proteins were identified using an anti-His_6 antibody. Proteins were cleaved from their His_6 tags by incubating bacterial lysates with biotinylated thrombin (Novagen), and thrombin was removed with streptavidin-agarose (Novagen). Cleavage was monitored by immunoblotting using anti-His_6, and Ab142 or Ab1.1 antisera for the NT and IBC fragments, respectively (Supplementary Fig. 4 online and Supplementary Methods online).

Europe PMC Funders Author Manuscripts

Europe PMC Funders Author Manuscripts

Purification of IP_3R1 from rat cerebellum

IP_3R1 was purified at 4°C from cerebella of adult rats using heparin-affinity chromatography44. Frozen cerebella were homogenized in homogenization medium (HM: 1M NaCl, 1mM EDTA, 50mM Tris, 1mM benzamidine, protease inhibitor cocktail tablet (Roche), pH 8.3) and centrifuged (100,000x*g*, 30min). The pellet was solubilized in HM without NaCl and supplemented with 1.2% CHAPS. After centrifugation (100,000x*g*, 1h), the NaCl concentration of the supernatant was increased to 250mM before loading onto heparin-agarose beads (Sigma). After 30min, the beads were washed twice in glycerol-containing medium (250mM NaCl, 50mM Tris, 10% glycerol, 1mM 2-mercaptoethanol, 1mM benzamidine, 1mM EGTA, 1% CHAPS, protease inhibitor cocktail, pH 8.0). IP_3R were then eluted with elution medium (500mM NaCl, 50mM Tris, 10% glycerol, 1mM 2-mercaptoethanol, 1mM benzamidine, 1mM EGTA, 50mM Tris, 1% CHAPS, pH 8.0), and aliquots frozen in liquid nitrogen before storage at -80°C.

^3H-IP_3 binding

Equilibrium-competition binding assays were performed at 4°C for 5min in TEM containing ^3H-IP_3 (18-23Ci/mmol, 0.2-1.5nM), bacterial lysate (5-10μg) or purified IP_3R (2.5μg), and competing ligands. Results were analysed by fitting to a Hill equation (GraphPad Prism) from which the IC_{50}, and thereby the K_d, were calculated. The variance of the ratios of mean values (a and b) were calculated from the variances (var) of each45: $\mathrm{var}(a/b) = (a/b)^2[(\mathrm{var}(a)/a^2)+(\mathrm{var}(b)/b^2)]$.

Single channel recording

Patch-clamp recording from excised nuclear patches of DT40 cells used the methods reported previously26,27. IP_3R are relatively non-selective cation channels (P_{Ba}/P_K ~6)1. K^+ Ba was therefore used as charge-carrier to increase single channel current amplitudes26 and avoid feedback regulation of IP_3R by permeating Ca^{2+}. QuB (http://www.qub.buffalo.edu) was used for analysis of all channel records (Supplementary Methods online).

Molecular modelling

We developed a model of the IBC-SD relationship from the coordinate files for the IBC (1N4K) and SD (1XZZ) using protein-protein docking. Coarse-grained models of the complex were first produced using the program Hex5.1 (http://www.csd.abdn.ac.uk/hex/)46. From these models we selected those in which the linked termini of the SD and IBC were appropriately separated, and then considered only those models in which residues from the SD known to affect binding of IP_3 to the IBC28,33 were located at an IBC-SD interface. A representative structure was further refined using a local docking search with RosettaDock47. Detailed methods are given in Supplementary Methods online. Our predicted structure of the IBC-SD complex (Fig. 5a,b and Supplementary Fig. 3 online) has an inertial radius of gyration (26.1Å), which is compatible with the Guinier radius of gyration (30.7Å) obtained by small angle X-ray scattering34.

Supplementary Material

Refer to Web version on PubMed Central for supplementary material.

Acknowledgments

We thank S. Dedos, P. da Fonseca, A. Burgen, S. Otto and M. Garcia Alai for helpful comments, and T. Woodman for advice on NMR spectroscopy. Supported by grants from the Wellcome Trust (to CWT, AMR (Bath) and BVLP)

and the Biotechnology and Biological Sciences Research Council (to CWT). AMR (Cambridge) holds a Junior Research Fellowship at Queens' College, Cambridge.

References

1. Foskett JK, White C, Cheung KH, Mak DO. Inositol trisphosphate receptor Ca^{2+} release channels. Physiol. Rev. 2007; 87:593–658. [PubMed: 17429043]
2. MacKinnon R. Potassium channels and the atomic basis of selective ion conduction (Nobel Lecture). Angew. Chem. Int. Edn. Engl. 2004; 43:4265–4277.
3. Bosanac I, et al. Structure of the inositol 1,4,5-trisphosphate receptor binding core in complex with its ligand. Nature. 2002; 420:696–701. [PubMed: 12442173]
4. Uchida K, Miyauchi H, Furuichi T, Michikawa T, Mikoshiba K. Critical regions for activation gating of the inositol 1,4,5-trisphosphate receptor. J. Biol. Chem. 2003; 278:16551–16560. [PubMed: 12621039]
5. Szlufcik K, et al. The suppressor domain of inositol 1,4,5-trisphosphate receptor plays an essential role in the protection against apoptosis. Cell Calcium. 2006; 39:325–336. [PubMed: 16458354]
6. Taylor CW, da Fonseca PCA, Morris EP. IP_3 receptors: the search for structure. Trends Biochem. Sci. 2004; 29:210–219. [PubMed: 15082315]
7. Lape R, Colquhoun D, Sivilotti LG. On the nature of partial agonism in the nicotinic receptor superfamily. Nature. 2008; 454:722–727. [PubMed: 18633353]
8. Auerbach A. Gating of acetylcholine receptor channels: Brownian motion across a broad transition state. Proc. Natl. Acad. Sci. USA. 2005; 102:1408–1412. [PubMed: 15665102]
9. Monod J, Wyman J, Changeux JP. On the nature of allosteric transitions: a plausible model. J. Mol. Biol. 1965; 12:88–118. [PubMed: 14343300]
10. Colquhoun D. Binding, gating, affinity and efficacy. Br. J. Pharmacol. 1998; 125:923–947.
11. Stephenson RP. A modification of receptor theory. Br. J. Pharmacol. 1956; 11:379–393.
12. Jin R, Banke TG, Mayer ML, Traynelis SF, Gouax E. Structural basis for partial agonist action at ionotropic glutamate receptors. Nature Neurosci. 2003; 6:803–810. [PubMed: 12872125]
13. Mayer ML. Glutamate receptors at atomic resolution. Nature. 2006; 440:456–462. [PubMed: 16554805]
14. Banke TG, Traynelis SF. Activation of NR1/NR2B NMDA receptors. Nature Neurosci. 2003; 6:144–152. [PubMed: 12524545]
15. Popescu G, Auerbach A. Modal gating of NMDA receptors and the shape of their synaptic response. Nature Neurosci. 2003; 6:476–483. [PubMed: 12679783]
16. Jencks WP. Binding energy, specificity, and enzymic catalysis: the circe effect. Adv. Enzymol. 1975; 43:219–410. [PubMed: 892]
17. Burgen ASV. Conformational changes and drug action. Fed. Proc. 1981; 40:2723–2728. [PubMed: 7297703]
18. Potter BVL, Lampe D. Chemistry of inositol lipid mediated cellular signaling. Angew. Chem. Int. Edn. Engl. 1995; 34:1933–1972.
19. Riley AM, Laude AJ, Taylor CW, Potter BVL. Dimers of D-*myo*-inositol 1,4,5-trisphosphate: design, synthesis, and interaction with $Ins(1,4,5)P_3$ receptors. Bioconj. Chem. 2004; 15:278–289.
20. Riley AM, et al. Interactions of inositol 1,4,5-trisphosphate (IP_3) receptors with synthetic poly(ethylene glycol)-linked dimers of IP_3 suggest close spacing of IP_3-binding sites. J. Biol. Chem. 2002; 277:40290–40295. [PubMed: 12183463]
21. Kramer RH, Karpen JW. Spanning binding sites on allosteric proteins with polymer-linked ligand dimers. Nature. 1998; 395:710–713. [PubMed: 9790193]
22. Poinas A, et al. Study of the interaction of the catalytic domain of $Ins(1,4,5)P_3$ 3-kinase A with inositol phosphate analogues. ChemBioChem. 2005; 6:1449–1457. [PubMed: 15997461]
23. Riley AM, Dozol H, Spiess B, Potter BVL. 2-*O*-(2-aminoethyl)-myo-inositol 1,4,5-trisphosphate as a novel ligand for conjugation: physicochemical properties and synthesis of a new $Ins(1,4,5)P_3$ affinity matrix. Biochem. Biophys. Res. Commun. 2004; 318:444–452. [PubMed: 15120621]

Europe PMC Funders Author Manuscripts
Europe PMC Funders Author Manuscripts

Europe PMC Funders Author Manuscripts

24. Tovey SC, Sun Y, Taylor CW. Rapid functional assays of intracellular Ca^{2+} channels. Nature Protocols. 2006; 1:258–262.
25. Takahashi M, Tanzawa K, Takahashi S. Adenophostins, newly discovered metabolites of *Penicillium brevicompactum*, act as potent agonists of the inositol 1,4,5-trisphosphate receptor. J. Biol. Chem. 1994; 269:369–372. [PubMed: 8276820]
26. Dellis O, et al. Ca^{2+} entry through plasma membrane IP_3 receptors. Science. 2006; 313:229–233. [PubMed: 16840702]
27. Rahman T-U, Skupin A, Falcke M, Taylor CW. Clustering of IP_3 receptors by IP_3 retunes their regulation by IP_3 and Ca^{2+} Nature. 2009; 458:655–659. [PubMed: 19348050]
28. Iwai M, Michikawa T, Bosanac I, Ikura M, Mikoshiba K. Molecular basis of the isoform-specific ligand-binding affinity of inositol 1,4,5-trisphosphate receptors. J. Biol. Chem. 2007; 282:12755–12764. [PubMed: 17327232]
29. Yoshikawa F, et al. Mutational analysis of the ligand binding site of the inositol 1,4,5-trisphosphate receptor. J. Biol. Chem. 1996; 271:18277–18284. [PubMed: 8663526]
30. Williams DH, Zhou M, Stephens E. Ligand binding energy and enzyme efficiency from reductions in protein dynamics. J. Mol. Biol. 2006; 355:760–767. [PubMed: 16325850]
31. Boehning D, Joseph SK. Direct association of ligand-binding and pore domains in homo- and heterotetrameric inositol 1,4,5-trisphosphate receptors. EMBO J. 2000; 19:5450–5459. [PubMed: 11032812]
32. Schug ZT, Joseph SK. The role of the S4-S5 linker and C-terminal tail in inositol 1,4,5-trisphosphate receptor function. J. Biol. Chem. 2006; 281:24431–24440. [PubMed: 16815846]
33. Bosanac I, et al. Crystal structure of the ligand binding suppressor domain of type 1 inositol 1,4,5-trisphosphate receptor. Mol. Cell. 2005; 17:193–203. [PubMed: 15664189]
34. Chan J, et al. Ligand-induced conformational changes via flexible linkers in the amino-terminal region of the inositol 1,4,5-trisphosphate receptor. J. Mol. Biol. 2007; 373:1269–1280. [PubMed: 17915250]
35. Kobilka BK, Deupi X. Conformational complexity of G-protein-coupled receptors. Trends Pharmacol. Sci. 2007; 28:397–406. [PubMed: 17629961]
36. Bosanac I, Michikawa T, Mikoshiba K, Ikura M. Structural insights into the regulatory mechanism of IP_3 receptor. Biochim. Biophys. Acta. 2004; 1742:89–102. [PubMed: 15590059]
37. George CH, Jundi H, Thomas NL, Fry DL, Lai FA. Ryanodine receptors and ventricular arrhythmias: emerging trends in mutations, mechanisms and therapies. J. Mol. Cell. Cardiol. 2007; 42:34–50. [PubMed: 17081562]
38. Wagenknecht T, Samsó M. Three-dimensional reconstruction of ryanodine receptors. Front. Biosci. 2002; 7:1464–1474.
39. Marwood RD, Correa V, Taylor CW, Potter BVL. Synthesis of adenophostin A. Tetrahedron: Asymmetry. 2000; 11:397–403.
40. Riley AM, et al. Scyllo-inositol pentakisphosphate as an analogue of myo-inositol 1,3,4,5,6-pentakisphosphate: chemical synthesis, physicochemistry and biological applications. ChemBioChem. 2006; 7:1114–1122. [PubMed: 16755629]
41. Sugawara H, Kurosaki M, Takata M, Kurosaki T. Genetic evidence for involvement of type 1, type 2 and type 3 inositol 1,4,5-trisphosphate receptors in signal transduction through the B-cell antigen receptor. EMBO J. 1997; 16:3078–3088. [PubMed: 9214625]
42. Cardy TJA, Traynor D, Taylor CW. Differential regulation of types 1 and 3 inositol trisphosphate receptors by cytosolic Ca^{2+} Biochem. J. 1997; 328:785–793. [PubMed: 9396721]
43. Yoshikawa F, et al. High efficient expression of the functional ligand binding site of the inositol 1,4,5-trisphosphate receptor in *Escherichia coli*. Biochem. Biophys. Res. Commun. 1999; 257:792–797. [PubMed: 10208862]
44. Jiang Q-X, Thrower EC, Chester DW, Ehrlich BE, Sigworth FJ. Three-dimensional structure of the type 1 inositol 1,4,5-trisphosphate receptor at 24 Å resolution. EMBO J. 2002; 21:3575–3581. [PubMed: 12110570]
45. Colquhoun, D. Lectures in biostatistics. Clarendon Press; Oxford: 1971.

46. Ritchie DW, Kozakov D, Vajda S. Accelerating and focusing protein-protein docking correlations using multi-dimensional rotational FFT generating functions. Bioinform. 2008; 24:1865–1873.
47. Gray JJ, et al. Protein-protein docking with simultaneous optimization of rigid-body displacement and side-chain conformations. J. Mol. Biol. 2003; 331:281–299. [PubMed: 12875852]
48. Riley AM, Correa V, Mahon MF, Taylor CW, Potter BVL. Bicyclic analogues of D-myo-inositol 1,4,5-trisphosphate related to adenophostin A: synthesis and biological activity. J. Med. Chem. 2001; 44:2108–2117. [PubMed: 11405648]
49. Riley AM, Guédat P, Schlewer G, Spiess B, Potter BVL. A conformationally restricted cyclic phosphate analogue of inositol trisphosphate: synthesis and physicochemical properties. J. Org. Chem. 1998; 63:295–305.
50. Riley AM, Potter BVL. Poly(ethylene glycol)-linked dimers of D-*myo*-inositol 1,4,5-trisphosphate. Chem. Commun. 2000:983–984.

Europe PMC Funders Author Manuscripts
Europe PMC Funders Author Manuscripts

Europe PMC Funders Author Manuscripts

Europe PMC Funders Author Manuscripts

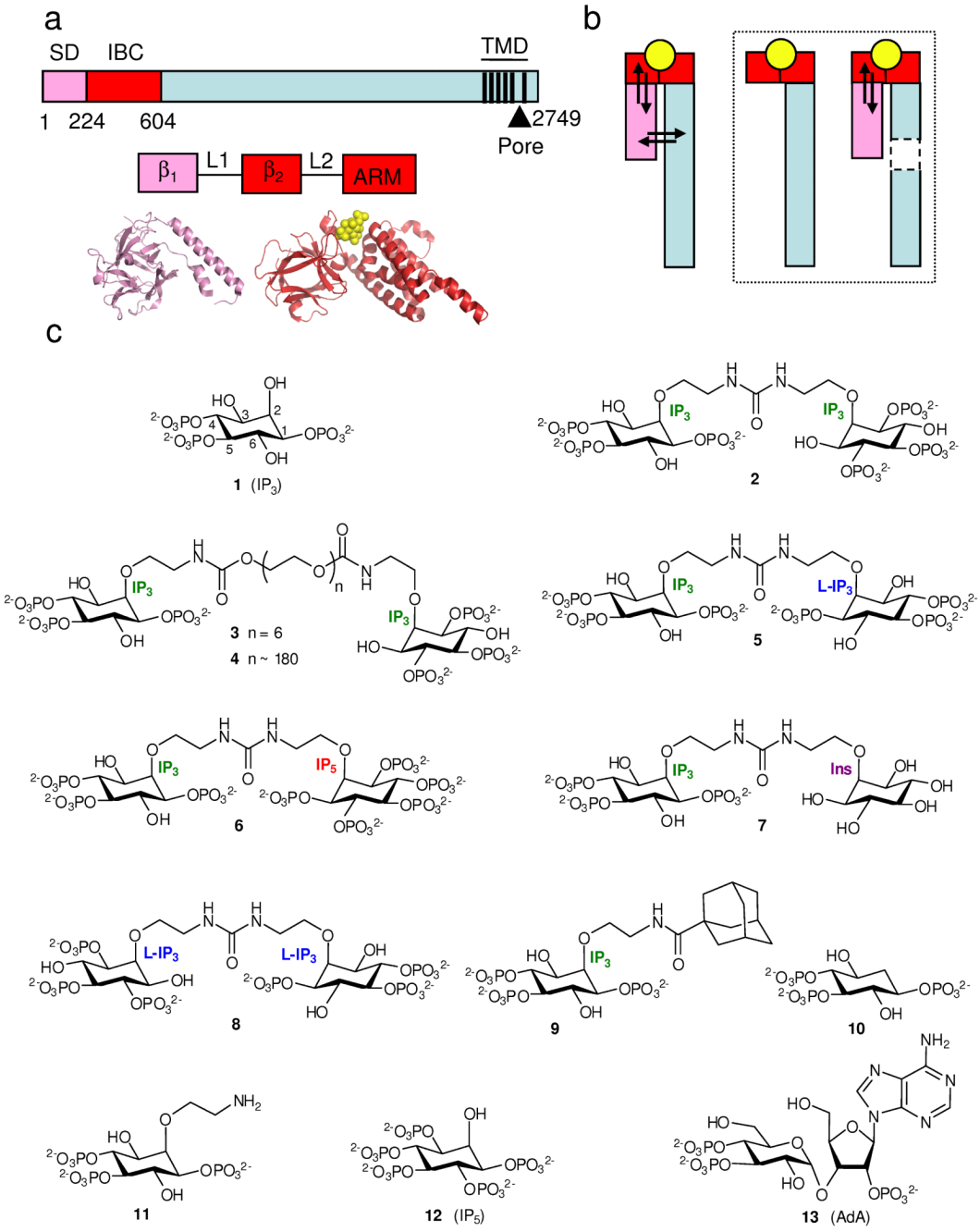

Figure 1.

Structure of the IP_3R and its ligands. (**a**) Key domains of IP_3R (numbering from rat IP_3R1, accession code NM_001007235). Pink denotes the SD (residues 1-223), red the IBC (224-604), and black vertical lines represent TMD. The SD (β_1) and IBC (β_2 and armadillo-like repeat, ARM) comprise 3 stably folded domains connected by flexible linkers (L1 and L2)34. Crystal structures are shown below3,33. (**b**) Agonist binding (yellow) to a discrete site on the receptor (IBC for IP_3R, red) evokes conformational changes that propagate through the receptor and which then affect (arrows) the binding site. Removal (boxed diagrams) of a domain through which conformational changes must pass prevents this

energetic interplay between conformational changes and binding. (**c**) Structures of the ligands used.

Europe PMC Funders Author Manuscripts

Europe PMC Funders Author Manuscripts

Europe PMC Funders Author Manuscripts

Europe PMC Funders Author Manuscripts

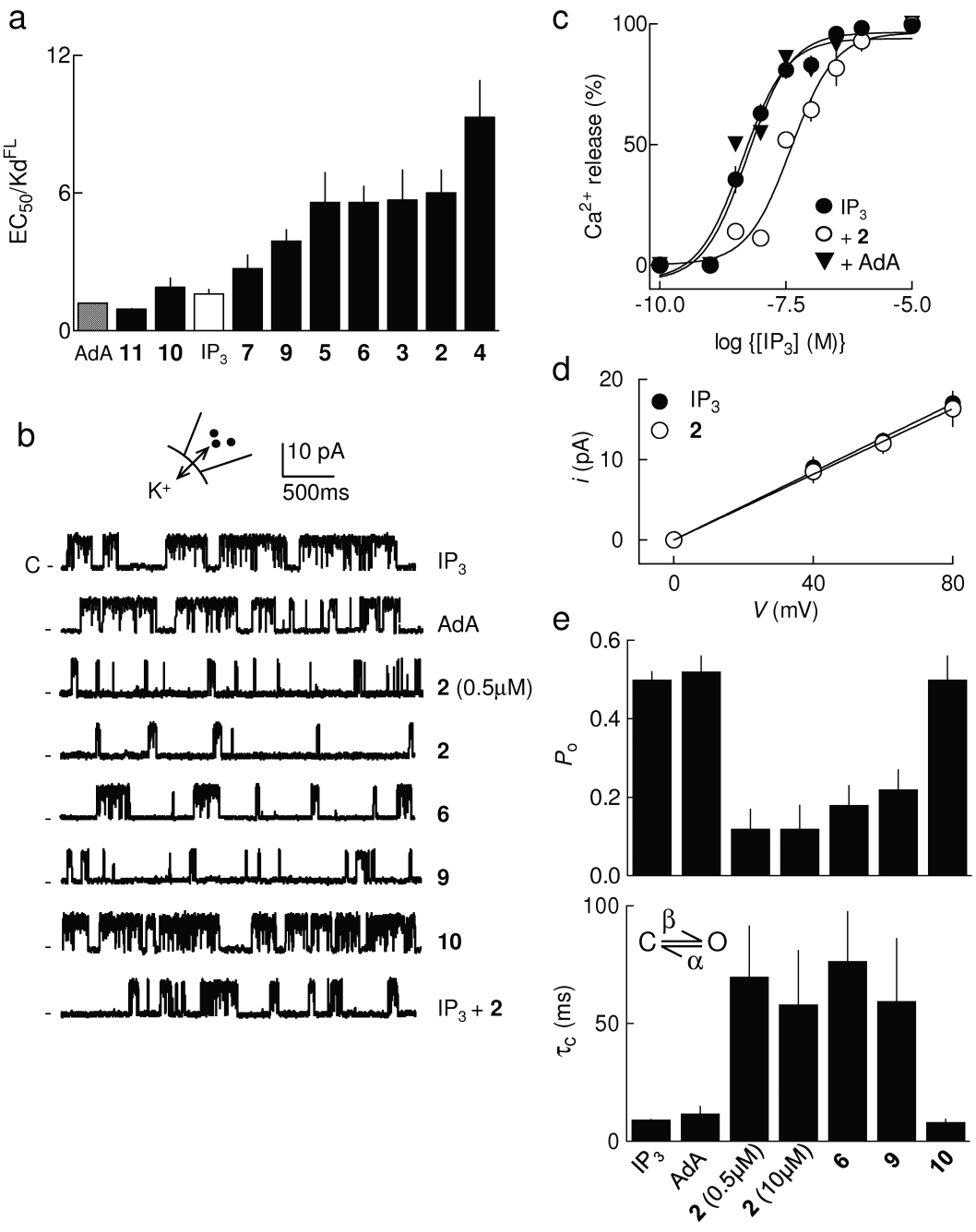

Figure 2.

2-*O*-modified IP_3 analogues are partial agonists of IP_3R. (**a**) From experiments similar to those shown in Supplementary Fig. 1a,b online, EC_{50}/K_d ratios ($n \geq 4$) were calculated for each ligand. (**b**) Traces (each typical of at least 3 similar records) show excised nuclear patch-clamp recordings from DT40-IP_3R1 cells with the pipette solution containing ATP (0.5mM), a free [Ca^{2+}] of 200nM and the indicated ligands (10μM, except where shown otherwise). The holding potential was +40mV. C denotes the closed state. (**c**) Cells were treated with IP_3 alone, or for 30s with either 0.1nM AdA or **2** and then with the indicated concentrations of IP_3. Results (n = 3) show the concentration-dependent release of Ca^{2+} by

IP_3. (**d**) Current-voltage (*i-V*) relationship for patches stimulated with IP_3 or **2** (means ± SEM, n = 3). (**e**) Summary data showing P_o and mean closed time (τ_c) for IP_3R1 stimulated as shown, n = 3-11 (further details in Supplementary Table 1 online). The simplified activation scheme for IP_3R shows the transition between closed (C) and open (O) states determined by rate constants, β and α (see Supplementary Methods online). All results (a,c-e) are means ± SEM.

Europe PMC Funders Author Manuscripts

Europe PMC Funders Author Manuscripts

Europe PMC Funders Author Manuscripts

Europe PMC Funders Author Manuscripts

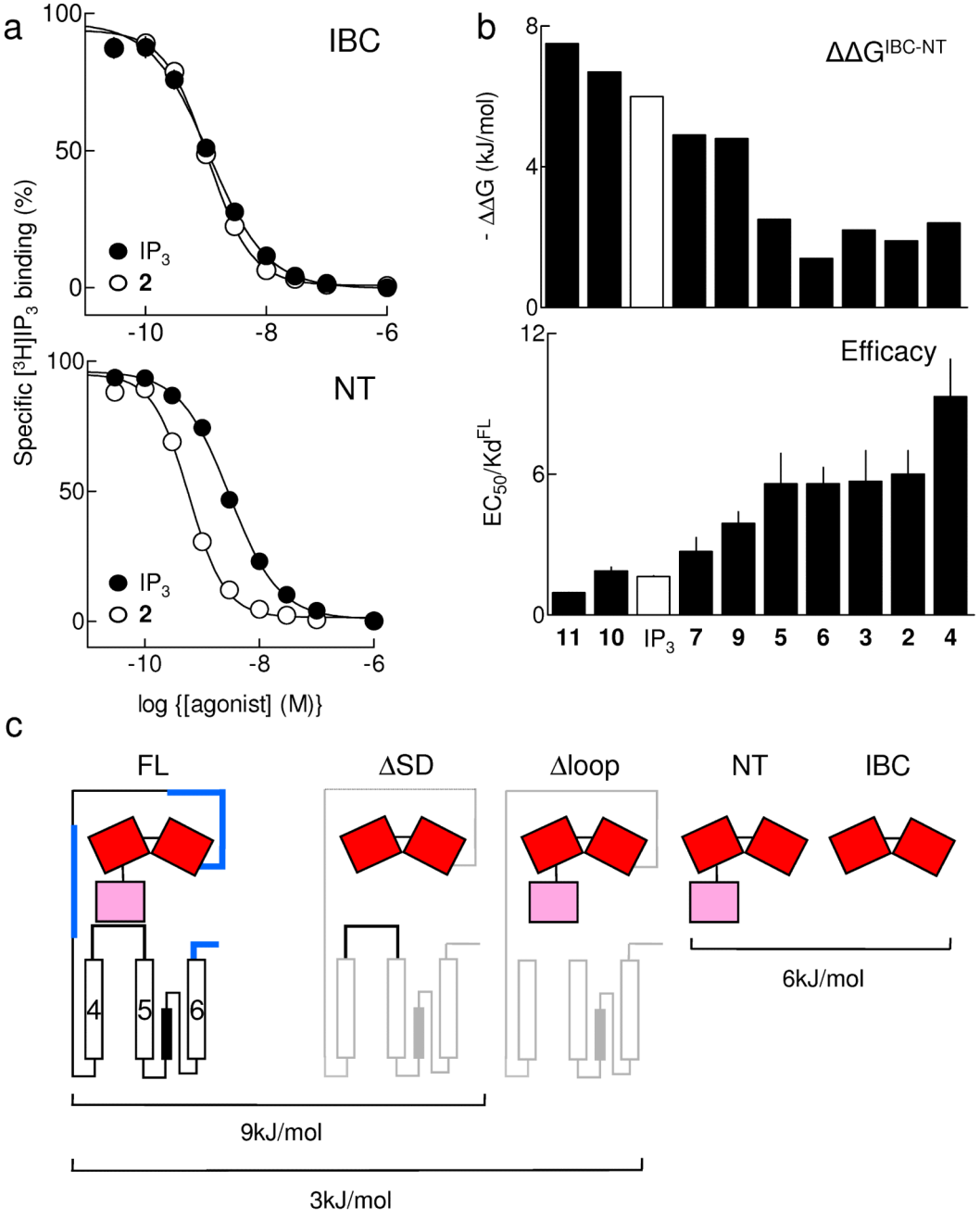

Figure 3.

Partial agonists are IP_3-like in their interactions with the IBC. (**a)** Equilibrium-competition binding to IBC (top) and NT (bottom) with ^{3}H-IP_3 and either IP_3 or **2**, n ≥ 17. (**b**) ΔΔG (ΔG^{IBC}-ΔG^{NT}), reflecting ΔG used to rearrange the IBC-SD relationship, is shown for each ligand, and compared with the efficacy of each (EC_{50}/K_d, with K_d determined for full-length IP_3R1). Results (a,b) are means ± SEM. **(c)** Estimated ΔG for conformational changes associated with IP_3R activation. The affinity (K_d) of IP_3 for IP_3R1 truncated as shown was measured herein (Table 1) or by others: by4 for ΔSD (IP_3R1 lacking residues 1-223), and by32 for Δloop (IP_3R1 lacking residues 2428-2437); ΔG was then calculated from $\Delta G = -RT\ln K_d$. The K_d for IP_3 was not directly measured in32, but under the conditions used the 4-

fold increase in IP_3 binding after deletion of residues 2428-2437 (ie Δloop) is likely to reflect a 4-fold decrease in K_d. We assume that deletion of IP_3R fragments through which conformational changes must pass increases IP_3 affinity because less binding energy is diverted into re-arranging the protein (Fig. 1b). Deletions of many other regions (shown in blue) do not increase IP_3 affinity4, suggesting that the IP_3-evoked conformational changes do not pass through them. This analysis is consistent with each IP_3 binding event diverting ~9kJ/mol into conformational changes of the IP_3R, of which ~6kJ/mol rearranges the SD-IBC relationship, and ~3kJ/mol is used by the SD to gate the pore.

Europe PMC Funders Author Manuscripts

Europe PMC Funders Author Manuscripts

Europe PMC Funders Author Manuscripts

Europe PMC Funders Author Manuscripts

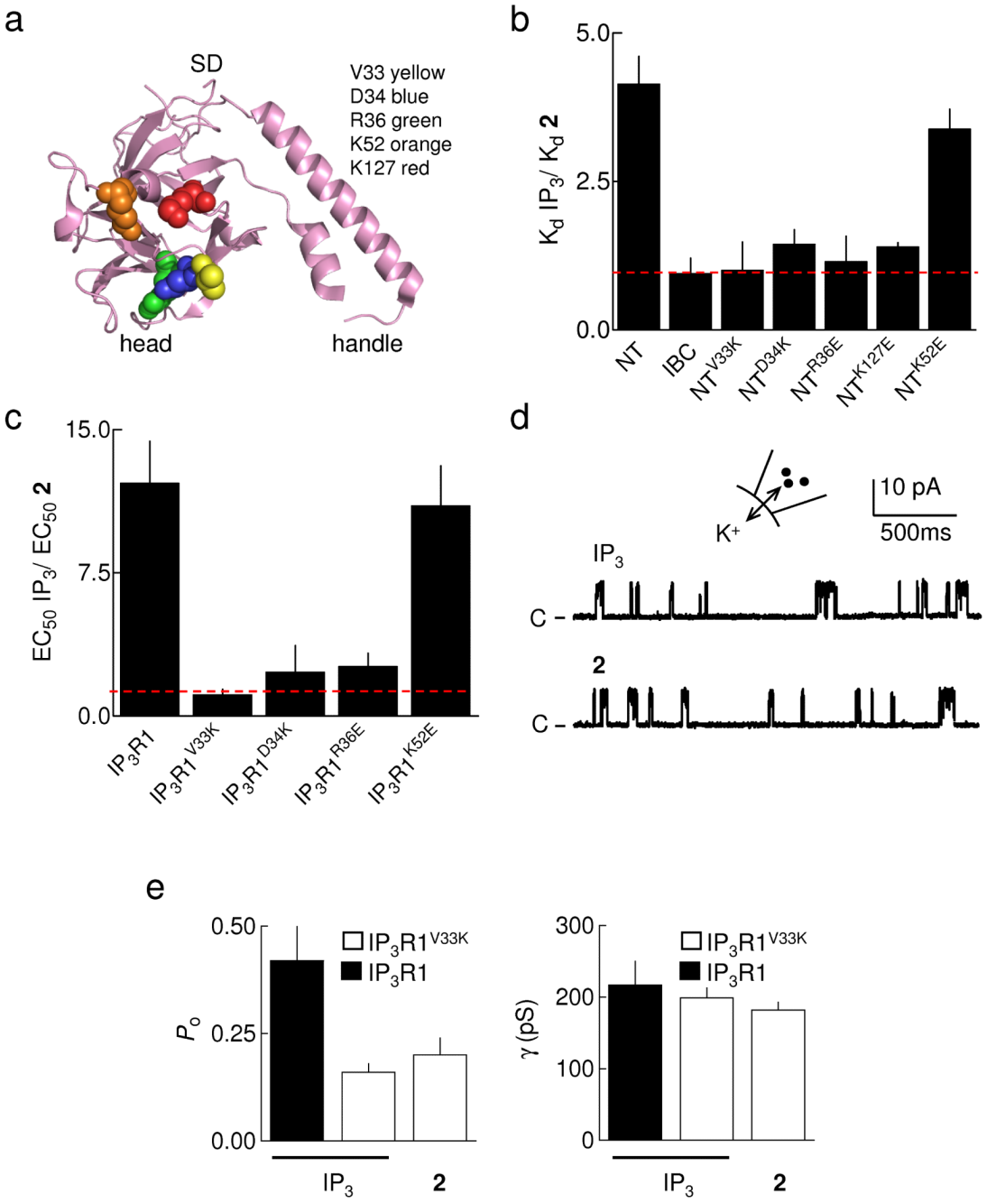

Figure 4.

Point mutations within the SD mimic partial agonists. (**a**) The structure of the SD33 is shown highlighting the residues mutated in this study. (**b**) Relative affinities (K_d) of IP_3 and **2** for IBC, NT, and NT with the indicated mutations (Supplementary Table 3 online); n ≥ 5. The dashed line shows K_dIP_3/K_d**2** = 1. (**c**) Potency (EC_{50}) of IP_3 relative to **2** in releasing Ca^{2+} from permeabilized DT40 cells stably expressing mutant IP_3R1 (Supplementary Table 4 online); n ≥ 5. The dashed line shows $EC_{50}IP_3/EC_{50}$**2** = 1. (**d**) Typical recordings from excised nuclear patches of DT40-IP_3R1^{V33K} cells with 10μM IP_3 or **2** in the patch pipette. The holding potential was +40mV. C denotes the closed state. (**e**) Summary data showing P_o

and γ_K for IP_3R1 and IP_3R1^{V33K} stimulated with 10μM IP_3 or **2**; n ≥ 3. Results (b,c,e) are means ± SEM.

Europe PMC Funders Author Manuscripts

Europe PMC Funders Author Manuscripts

Europe PMC Funders Author Manuscripts

Europe PMC Funders Author Manuscripts

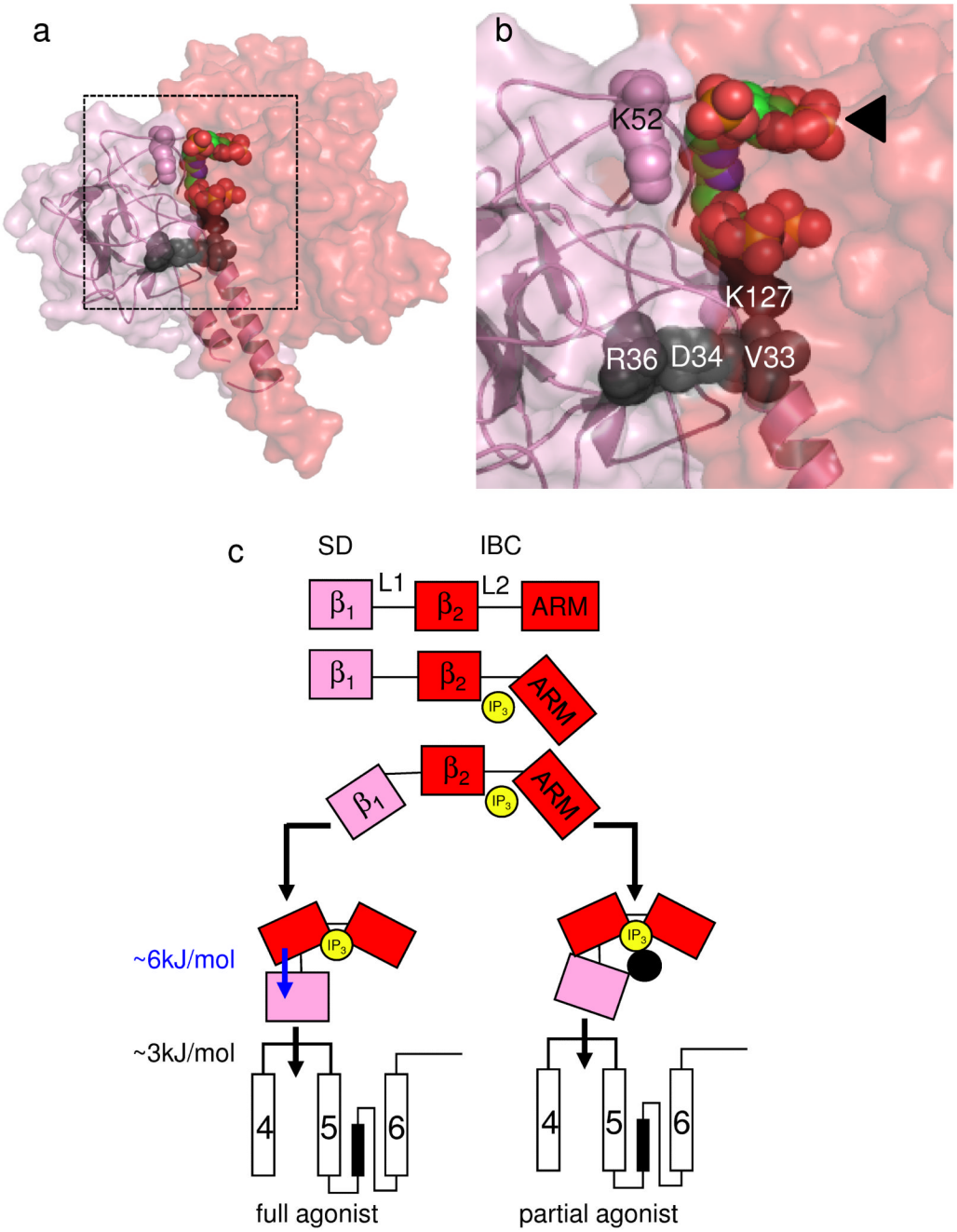

Figure 5.

IP_3 binding to the IBC activates IP_3R entirely via the SD. (**a,b**) Predicted relationship between the SD (pink) and IBC (red) with **2** bound. Residues within the SD that affect efficacy (V33, D34, R36 and K127) are shown in black (see Fig. 4a and Supplementary Fig. 3 online for details). The ineffective residue K52 is shown in pink. Panel b is an enlargement of the boxed area in panel a, with the IBC-bound IP_3 moiety indicated by an arrow. (**c**) IP_3 (yellow) rearranges the 2 domains of the IBC (β_2 and ARM, red) around its L2 loop causing rearrangement of the SD (= β_1, pink) around the L1 loop. The SD is then entirely responsible for transmitting conformational changes towards the pore, probably by directly interacting with the TMD4-5 loop of an adjacent subunit31,32. ΔG associated with

rearranging the SD and its subsequent communication with the pore region is shown. Partial agonists effectively rearrange the IBC, but the inositol 2-*O*-substituent (or point mutations in the SD; black circle) disrupt the IBC-SD interface and so block communication with the SD. The latter is now less likely to contact the TMD4-5 loop, but once it makes contact the channel gates normally.

Europe PMC Funders Author Manuscripts

Europe PMC Funders Author Manuscripts

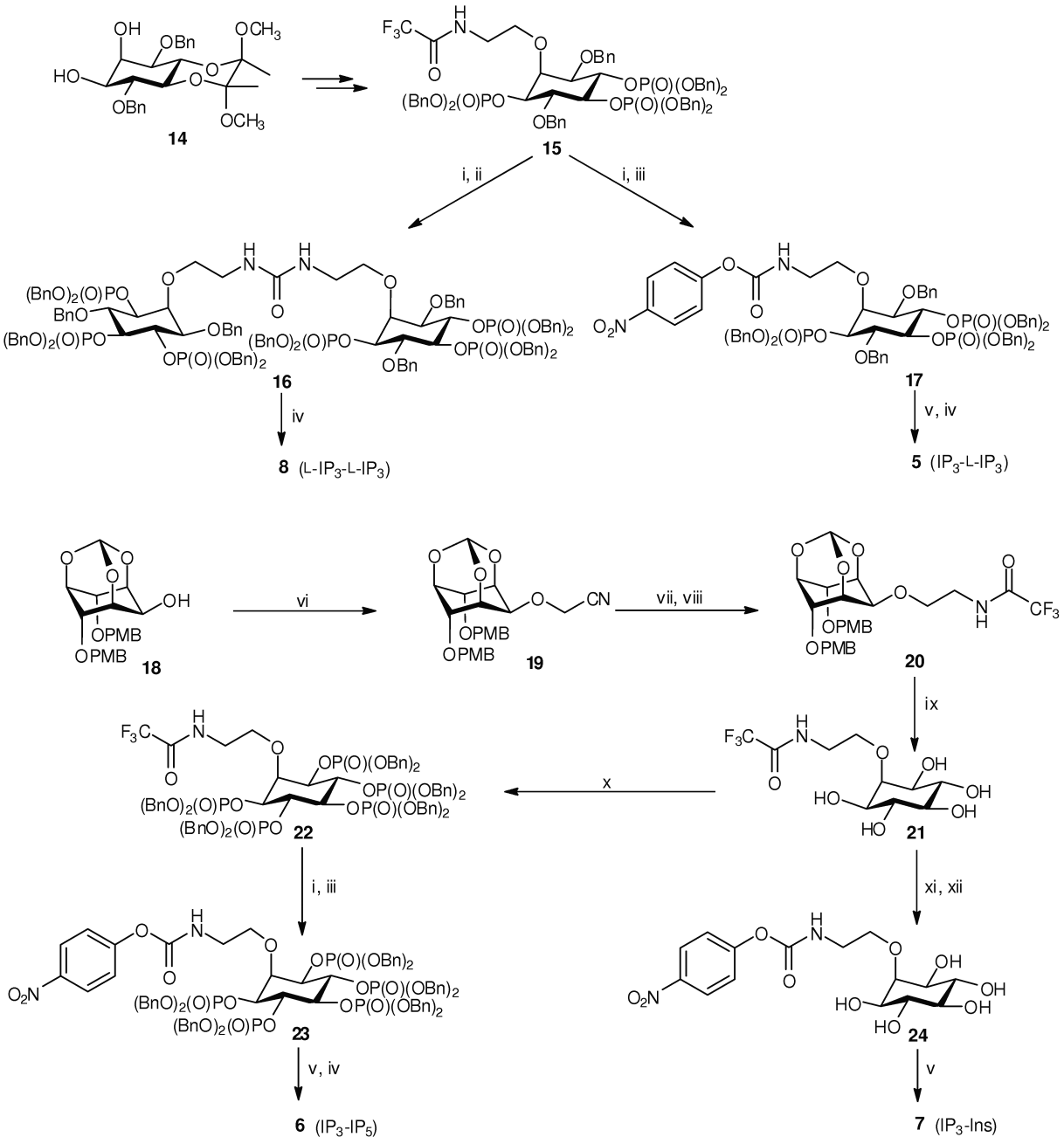

Scheme 1.

Syntheses of hetero-dimers **5, 6** and **7**, and L-IP_3 dimer **8**. Dimers **5** and **8** were synthesized from L-IP_3-based building block **15**, obtained from diol **14**48 (see Supplementary Methods online). The *N*-trifluoroacetyl protecting group was removed, generating an unstable amine which was reacted with 0.5 equivalents of bis(4-nitrophenyl) carbonate, giving protected L-IP_3 dimer **16**. Hydrogenolytic deprotection of **16** gave L-IP_3 dimer **8**. When 1 equivalent of bis(4-nitrophenyl) carbonate was used, the product was 4-nitrophenyl *N*-alkylcarbamate **17**, which could be isolated and conjugated with D-IP_3 component **11**. The conjugation reaction was carried out in CD_3OD and monitored by ^{31}P NMR spectroscopy. Deprotection followed

Europe PMC Funders Author Manuscripts
Europe PMC Funders Author Manuscripts

by anion-exchange chromatography then gave IP_3–L-IP_3 hetero-dimer **5**. Dimers **6** and **7** were synthesized from alcohol **18**49. Nitrile **19** was reduced, and the amine product was temporarily protected as the *N*-trifluoroacetamide (**20**). Acid-labile protecting groups were then removed, giving pentaol **21**, which was converted, via **22**, into carbamate **23**. Carbamate **23** was then conjugated with **11**, and deprotection followed by anion-exchange chromatography gave IP_3–IP_5 hetero-dimer **6**. Alternatively, conjugation of carbamate **24** with **11** gave IP_3–Ins dimer **7**. Reagents and conditions: (i) LiOH, THF, MeOH, H_2O; (ii) bis(4-nitrophenyl) carbonate (0.5 equiv), THF; (iii) bis(4-nitrophenyl) carbonate (1 equiv), THF; (iv) H_2, $Pd(OH)_2$/C, MeOH, H_2O; (v) **11**, CD_3OD, Et_3N; (vi) NaH, $BrCH_2CN$, CH_3CN; (vii) $LiAlH_4$, THF; (viii) $EtOC(O)CF_3$, THF; (ix) TFA, H_2O; (x) $(BnO)_2PN^iPr_2$, 1*H*-tetrazole, CH_2Cl_2 then 3-chloroperoxybenzoic acid; (xi) Et_3N, H_2O, reflux; (xii) bis(4-nitrophenyl) carbonate (1 equiv), DMF, Et_3N. Bn, benzyl; PMB, 4-methoxybenzyl. All experimental procedures are described in detail in Supplementary Methods online.

Europe PMC Funders Author Manuscripts

Europe PMC Funders Author Manuscripts

Europe PMC Funders Author Manuscripts
Europe PMC Funders Author Manuscripts

Nat Chem Biol. Author manuscript; available in PMC 2010 May 13.

Table 1

Responses to IP_3 analogues. The effects of each analogue on Ca^{2+} release from the intracellular stores of permeabilized DT40-IP_3R1 cells and on ^3H-IP_3 binding to full-length purified IP_3R1 (FL), its N-terminal (NT, residues 1-604) or the IP_3-binding core (IBC, residues 224-604) are summarized (n ≥ 4). For dimers, the estimated separation of the two moieties is shown calculated as in50. Results are means ± SEM. *No detectable Ca^{2+} release with 30μM **8**. ND, not determined.

		Ca^{2+} release		FL		NT	IBC
		EC_{50} (nM)	Release %	K_d (nM)	EC_{50}/K_d	K_d (nM)	K_d (nM)
1	IP_3	20±2	77±5	12.5±1.06	1.6±0.2	2.82±0.26	0.21±0.03
13	AdA	1.5±0.1	75±6	1.26±0.11	1.2±0.01	ND	ND
2	$(IP_3)_2$ 0.8nm	2.7±0.4	76±6	0.45±0.04	6.0±1.0	0.41±0.03	0.18±0.01
3	$(IP_3)_2$ 1.5nm	4.9±0.3	74±6	0.86±0.19	5.7±1.3	0.47±0.09	0.18±0.01
4	$(IP_3)_2$ 8nm	13±1	73±7	1.39±0.23	9.3±1.6	1.37±0.20	0.48±0.02
5	IP_3–L-IP_3 0.8nm	5±1	70±7	0.90±0.12	5.6±1.3	0.42±0.02	0.14±0.02
6	IP_3–IP_5 0.8nm	5±0	72± 5	0.89±0.11	5.6±0.7	0.36±0.03	0.20±0.01
7	IP_3–Ins 0.8nm	21±1	76±4	7.82±1.73	2.7±0.6	2.81±0.22	0.33±0.01
8	$(L\text{-}IP_3)_2$ 0.8nm	Inactive*	ND	ND	ND	ND	ND
9	2-adamantane-IP_3	30±3	71±1	7.62±0.51	3.9±0.5	1.63±.022	0.20±0.02
10	2-deoxy-IP_3	32±7	65±3	17.1±1.1	1.9±0.4	4.01±0.38	0.22±0.03
11	2-aminoethyl-IP_3	42±5	69±6	43.6±4.6	0.95±0.02	13.5±2.0	0.52±0.04